

Faulty States can be used in Cat Code Error Correction

Michael Hanks,^{1,*} Soovin Lee,¹ Nicolo Lo Piparo,² Shin Nishio,^{2,3,4} William J. Munro,^{2,4} Kae Nemoto,^{2,4} and M.S. Kim¹

¹*Blackett Laboratory, Imperial College London, London SW7 2AZ, United Kingdom*

²*Okinawa Institute of Science and Technology Graduate University, 1919-1 Tancha, Onna-son, Kunigami-gun, Okinawa 904-0495, Japan*

³*Department of Informatics, School of Multidisciplinary Sciences, Sokendai (The Graduate University for Advanced Studies), 2-1-2 Hitotsubashi, Chiyoda-ku, Tokyo 101-8430 Japan*

⁴*National Institute of Informatics, 2-1-2 Hitotsubashi, Chiyoda-ku, Tokyo 101-8430, Japan*

Bosonic codes have seen a resurgence in interest for applications as varied as fault tolerant quantum architectures, quantum enhanced sensing, and entanglement distribution. Cat codes have been proposed as low-level elements in larger architectures, and the theory of rotationally symmetric codes more generally has been significantly expanded in the recent literature. The fault-tolerant preparation and maintenance of cat code states as a stand-alone quantum error correction scheme remains however limited by the need for robust state preparation and strong inter-mode interactions. In this work, we consider the teleportation-based correction circuit for cat code quantum error correction. We show that the class of acceptable ancillary states is broader than is typically acknowledged, and exploit this to propose the use of many-component “bridge” states which, though not themselves in the cat code space, are nonetheless capable of syndrome extraction in the regime where non-linear interactions are a limiting factor.

I. INTRODUCTION

Quantum enhanced devices promise significant performance improvements in a range of applications across computation [1–3], secure communication [4, 5], and metrology [6]. In recent years, the first proof-of-principle demonstrations of quantum advantage have been published [7, 8], initiating a period of competition between large quantum systems and high-performance classical computers [9–12]. It is widely thought, however, that to move beyond the proof-of-principle stage and into industrially relevant quantum information processing tasks will require circuits at least tens of thousands of gates deep [13] (and usually significantly more [2, 14, 15]). Further, the cost of a noisy quantum circuit is expected to scale exponentially in its depth [16, 17]: As the problems addressed by quantum-enhanced devices scale up, some form of quantum error correction [18, 19] will be required.

In most architectural proposals for quantum computation, the logical structure is that of a discrete qubit code [20–23]. Physical qubits typically occupy the lower levels of a system such as a trapped ion or superconducting circuit, while Bosonic modes and cavities may be present to enable tuneable coupling or readout. Some recent proposals have however inverted the idea of using harmonic modes to access finite dimensional Hilbert spaces, suggesting the use of systems such as cavity modes or the vibrational modes of trapped ions to encode information [24, 25]. Such modes could then be entangled together in a larger discrete lattice encoding [26–28]. It is also likely that large quantum devices will involve a modular or dis-

tributed structure, for which photonic carrier subsystems are a prime candidate in communication [29–31].

Around the turn of the century, it was noted by several authors [32–34] that one could realise discrete qudit codes in the phase space of one or several harmonic oscillator modes. Codes defined in such a discrete subspace (the ‘code’ or ‘logical qudit’ subspace) of a larger continuous-variable Hilbert space are known as Bosonic codes [35]. These are typically represented in phase space by a tiling of the space having a discrete (perhaps approximate) symmetry. The magnitude of the symmetry transformation defines a characteristic code distance. Here, we consider only single-mode Bosonic codes.

For Bosonic codes with discrete symmetries in the number–phase representation, measurement of the mean photon number modulo N can be made fault tolerant either via repetition of the non-destructive measurement circuit provided in [36] (and depicted in Figure 1), or with error detection and post-selection, as was proposed for GKP state preparation in [37]. So far, however, in the absence of code concatenation, teleportation-based error correction (“tele-correction”) [38, 39] appears to be the only reliable method for the measurement of rotation errors. This poses a challenge for fault tolerant state preparation [36]: The fault tolerance of the teleportation process relies not only on low-weight parity measurements with locally constrained errors, but on the preparation of high-fidelity encoded ancillary states.

Many methods have been proposed to generate two-component cat states, including nonlinear interactions [33, 40, 41], projective measurements [42–47], and reservoir engineering [48–50]. Methods to prepare more general multi-component cat code states are fewer, but tend to follow similar lines, exploiting either non-linear interactions [51–54], or interaction with and projective mea-

* m.hanks@imperial.ac.uk

surement of an ancillary system [55–57]. These methods are not natively robust against errors, however, and must be combined with active, measurement-based correction schemes [36, 58, 59].

Fault tolerance has not always been considered a necessary element in the preparation and maintenance of the code states. Several results for cat codes in the last several years have focussed on their role producing biased noise as a base layer in concatenated schemes for fault tolerant quantum computing architectures, with subsequent layers of concatenation making use of surface codes. In these settings, large-amplitude two-component code states are passively protected on the scale of the gate time either by a two-photon dissipative process [26, 60, 61] or by achieving fast gates via a large Kerr-nonlinearity [62]. Gottesman–Kitaev–Preskill (GKP) codes have also received particular attention for such concatenated schemes [63–67].

We consider the fault tolerant initialisation of the multi-component cat codes. To date the only method proposed in the literature of which we are aware makes use of code concatenation [36], requiring complex multi-mode entanglement. For ancillary state preparation with the surface code, resource advantages have been found by distilling noisy gates and introducing reduced earlier stages with post-selection [68, 69]. Here we propose an alternative to code concatenation for the preparation of ancillary cat code states, investigating the performance of a generalised Yurke–Stoler scheme provided by Lee et al. [54] for faulty state preparation as a primitive in this procedure.

II. THE CAT CODE

The cat code states were first introduced with two coherent state components by Cochrane et al. [33]. These states were subsequently generalised to incorporate the imaginary axis in phase space [70], and to fix logical qubit information in the relative phases [71], before finally being extended to superpositions with any number of coherent state components [59]. Cat codes have been used in landmark experimental demonstrations of encoded Bosonic qubits [72, 73]. The cat code states for a logical qubit may be defined either as a superposition of $2D$ coherent states,

$$|\mu_{\alpha,D}\rangle = \frac{1}{2D\sqrt{\mathcal{N}_{\mu,\alpha,D}}} \sum_{k=0}^{2D-1} e^{-i\pi k\mu} |e^{\frac{i\pi k}{D}}\alpha\rangle, \quad (1)$$

or in terms of Fock states as

$$|\mu_{\alpha,D}\rangle = \frac{e^{-\frac{|\alpha|^2}{2}}}{\sqrt{\mathcal{N}_{\mu,\alpha,D}}} \sum_{m=0}^{\infty} \frac{\alpha^{(2m+\mu)D}}{\sqrt{((2m+\mu)D)!}} |(2m+\mu)D\rangle. \quad (2)$$

Here $\mu \in \{0, 1\}$, the normalisation constant is

$$\mathcal{N}_{\mu,\alpha,D} = e^{-|\alpha|^2} \sum_{m=0}^{\infty} \frac{|\alpha|^{2(2m+\mu)D}}{((2m+\mu)D)!}, \quad (3)$$

$\alpha \in \mathbb{R}_+$ is the cat code radius (the magnitude for coherent states equidistant around a circle in phase space) and $D \in \mathbb{N}_{>0}$ is the code distance, so that ideally the cat code can perfectly correct for up to $D-1$ lost photons. D is half the number of coherent state components and also the separation between Fock state components with non-zero population in an arbitrary logical state.

Cat codes may be stabilised passively via reservoir engineering [71, 74], but for large D the associated $2D$ -photon interactions become increasingly difficult to produce. We will be interested here in active measurement-based correction, specifically the tele-correction scheme [36, 58, 59].

A. Phase Measurement

The tele-correction circuit, shown in Figure 1 (a), can be used in the generation of rotationally symmetric Bosonic code states [36], including cat code states. This circuit involves measurement of the phase of the data qubit $|\psi\rangle_K$, which provides information not only about the logical state but also about perturbations due to error.

Measurement inefficiencies have been highlighted as a dominating source of noise in teleportation-based error correction circuits [75]. It was recently shown by Oh et al. [76] that a homodyne measurement is the optimal Gaussian measurement for the phase estimation problem, achieving a phase-independent sensitivity bound set by the quantum Fisher information. However, this measurement requires knowledge of an optimal quadrature angle, whereas multi-component cat code states can have an arbitrary degree of rotational symmetry. For the balanced heterodyne measurement, the angular dependence is removed, but at the cost of halving the Fisher information, and so doubling corresponding mean-squared error. While recent papers have considered adaptive homodyne measurements as an alternative [77], when the coherent state components of the code state are sufficiently separated heterodyne detection nonetheless remains as a practical choice offering a favourable compromise between performance and implementability.

The ancillary states used in the tele-correction procedure of Figure 1 (a) need not be $|+\rangle$ states. Suppose that, for known θ and m , an ancillary state differs from the logical $|+\rangle$ state by a rotation $e^{i\theta\hat{n}}$ about the origin and by an m -photon loss event \hat{a}^m . The anomalous rotation commutes with the controlled rotation gates of the tele-correction circuit, and can be accounted for by a rotation of the decision lines for the heterodyne measurements (see Figure 2). The anomalous photon loss event, affecting only the relative phases between coherent state

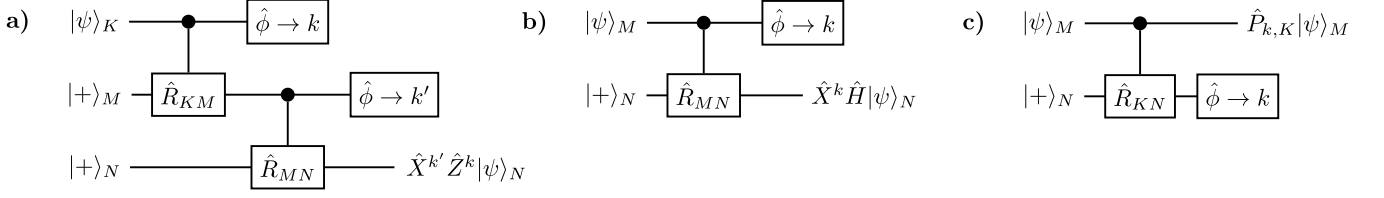


FIG. 1. **a)** Tele-correction circuit for rotationally symmetric Bosonic codes [36], including cat codes, for arbitrary encoded input state $|\psi\rangle_K$. Here the state subscripts K, M, N are even and denote the numbers of coherent state components in the encoding. \hat{R}_{MN} represents the controlled rotation gate: $e^{i(4\pi/MN)\hat{n}_1\hat{n}_2}$. Operators $\hat{\phi}$ denote general phase measurements, binned into indices k, k' by the nearest coherent state components — the pure output states shown here assume that components are perfectly distinguishable. **b)** Projective Hadamard circuit for rotation codes, which is repeated to form the full tele-correction circuit. **c)** Modular photon number measurement. Here $\hat{P}_{k,K}$ represents projection onto the subspace of photon numbers congruent to k modulo K , and the phase angle in this case is binned into K segments modulo $4\pi/N$.

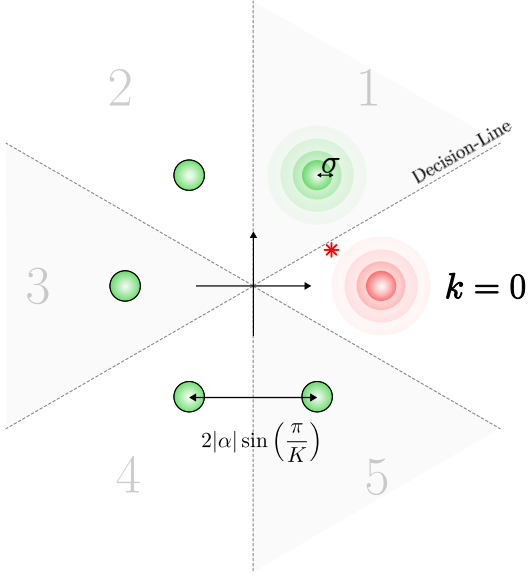


FIG. 2. Sketch of the binning procedure for heterodyne phase measurements in the tele-correction circuit of Figure 1 (a), with the number of components $K = 6$ and $k \in \{0 : K - 1\}$. For example, if the location indicated by heterodyne detection is given by the red asterisk, the nearest coherent state component would be represented by the red concentric circles, corresponding to index $k = 0$.

components, does not affect the measurement outcomes directly. It does however result in a correlated rotation for other ancillae on commutation through a controlled rotation gate. So long as m is a known parameter, the angle of this correlated rotation is also known and can be accounted for as mentioned above. These considerations amount to a qudit generalisation of Pauli-frame tracking, which has already been proposed for rotationally symmetric Bosonic codes [36] to allow for the random outcomes of the tele-correction and Hadamard circuits.

Assuming the code distance is large enough for heterodyne measurements to give accurate results, the final state of the tele-correction circuit in Figure 1 (a) is ap-

proximately

$$\frac{c_0}{\sqrt{2}} \left(|+\rangle_N + e^{-i\pi k'} |-\rangle_N \right) + \frac{c_1 e^{-i\pi k}}{\sqrt{2}} \left(|+\rangle_N - e^{-i\pi k'} |-\rangle_N \right), \quad (4)$$

where the input state is $|\psi\rangle_K = c_0|0\rangle_K + c_1|1\rangle_K$, while k, k' index the coherent state components inferred from the measurement outcomes, as sketched in Figure 2. An incorrect outcome in the first measurement would give an incorrect result for k , and likewise in the second measurement for k' . If these incorrect outcomes differ from the genuine result by an odd amount, then the inferred and actual states are orthogonal. False measurement outcomes must be suppressed by increasing α relative to K and M (the circumferential separation between coherent state components).

We can look at the probability of error in the final state to leading order by concentrating only on incorrect measurement outcomes with support on neighbouring coherent state components. The total variation distance (TVD) and associated single trial error p_{err} for distinguishing between two Gaussian distributions of equal variance are given by

$$\text{TVD} = \text{erf} \left(\frac{|\mu_1 - \mu_2|}{2\sqrt{2}\sigma} \right), \quad p_{\text{err}} = \frac{1 - \text{TVD}}{2}. \quad (5)$$

When the coherent state components are distributed evenly in phase space at $2D$ points around a circle of radius $|\alpha|$, the distance between two components $|\alpha\rangle$ and $|\alpha e^{i\frac{\pi}{2D}}\rangle$ is $2|\alpha| \sin(\frac{\pi}{2D})$, as shown in Figure 2. The total variation distance then becomes

$$\text{TVD}_{\alpha,D} = \text{erf} \left(\sqrt{2} |\alpha| \sin \left(\frac{\pi}{2D} \right) \right), \quad \approx 1 - e^{-\frac{1}{2} (2|\alpha| \sin(\frac{\pi}{2D}))^2}, \quad (6)$$

where the final line approximates the error function to only the first order term in the Bürmann expansion [78].

When the local oscillator of the heterodyne measurement is weak, the measurement error depends on the discrete lattice of heterodyne detection outcomes and must be determined numerically.

III. MANY-COMPONENT CAT STATES

Let us now look at generating high fidelity ancillary states using the Hadamard and modular photon number measurement circuits respectively depicted in Figure 1 (b) and (c). Since $|+\rangle_M$ corresponds to $|0\rangle_{M/2}$ [36], the simplest procedure is to use two input coherent states with controlled rotation $e^{i(4\pi/K)\hat{n}_1\hat{n}_2}$ in the modular photon number measurement circuit. This gives $\hat{a}^{K/2-k}|+\rangle_K$. When K is small, however, generating a non-linear interaction of sufficient strength to enact this controlled rotation may not be feasible. To address this issue, we introduce a many-component state in the central rail of the tele-correction circuit. Such a state may be prepared either by cross-Kerr interaction as described above or by self-Kerr non-linearity in a single field, which we consider next.

A. Generalised Yurke-Stoler Method

In 1994, Lee et al. [54] generalised the method of Yurke and Stoler [51] to generate multi-component circular cat states using Kerr non-linearities. The Hamiltonian required for this method,

$$\hat{H} = \hbar\omega\hat{n} + \hbar\lambda\hat{n}^2, \quad (7)$$

where \hat{n} is the photon number operator, involves a quadratic self-Kerr interaction in addition to the standard free energy of the mode. Lee et al. noted that at times t such that

$$t = \frac{\pi}{\lambda N}, \quad (8)$$

an N -component circular superposition of coherent states is obtained. This superposition takes the form

$$|\Psi\rangle = \frac{1}{\sqrt{N}} \sum_{m=1}^N e^{i\xi_m} |\alpha e^{i\phi_m}\rangle, \quad (9)$$

where \mathcal{N} is a normalisation constant, $e^{i\phi_m}$ are the N th roots of unity and the phases ξ_m are described below. We will refer to these as Yurke-Stoler (YS) states. The Hamiltonian only contains terms that preserve the photon number distribution. Consequently, the YS states do not have the modular photon number distribution characteristic of rotationally symmetric code states — the relative phases $e^{i\xi_m}$ are “incorrect”.

The relative phases of the coherent state components using the generalised YS method of generation are solu-

tions to the equation

$$\frac{1}{\sqrt{N}} \sum_{m=1}^N x_m e^{i2\pi k \frac{m}{N}} = e^{-i\pi\left(\frac{k^2}{N} + k\right)}, \quad (10)$$

with $x_m = e^{i\xi_m}$. We recognise that the relative phases then are the arguments of solutions to the discrete Fourier transform for the equation

$$e^{-i\pi\left(\frac{k^2}{N} + k\right)}, \quad (11)$$

which we identify as a linear chirp-signal [79]. The solution to the discrete Fourier transform gives us [80]

$$\xi_m = \frac{\pi}{4} \left[N \left(\frac{2m}{N} - 1 \right)^2 - 1 \right], \quad (12)$$

with $m \in \{0, 1, \dots, N-1\}$. It can be readily checked that for the cases $N \in \{2, 3, 4, 5\}$, these solutions correspond to those listed in [54].

1. Modular Photon Number Measurement

In the modular photon number measurement of Figure 1 (c), we are able to account for relative phases between coherent states in the probe subsystem. Using a coherent state $|\beta\rangle$ as the target input subsystem and a YS state of amplitude α as the probe, we have

$$\frac{1}{\sqrt{N}} \sum_{m=1}^N e^{i\xi_m} e^{-\frac{|\beta|^2}{2}} \sum_{n=0}^{\infty} \frac{\beta^n}{\sqrt{n!}} |n\rangle |-\alpha e^{i\phi_m} e^{-i4\pi \frac{n}{KN}}\rangle \quad (13)$$

after applying the controlled rotation gate. We observe that the relative phases on the coherent state components of the YS state are transferred sequentially to the Fock states in the modular photon number subspace. A second application of the self-Kerr interaction,

$$e^{i\frac{4\pi}{K^2N}\hat{n}^2}, \quad (14)$$

removes the quadratic dependence in ξ_m . The time required for this interaction is on the order of that for the generation of the YS states, and becomes shorter as the spacing between Fock states increases.

To demonstrate the stability of the modular photon number measurement against measurement error as we increase the number of coherent state components, in Figure 3 we sample measurement outcomes and the final state fidelities with a coherent state target input and cat state probe. Measurement outcomes are sampled randomly for circuits implementing photon number measurements mod 2 and mod 4. Final states with fidelities above 0.99 are observed with probability $p > 0.985$. The fidelity

$$F = |\langle\psi_{\text{actual}}|\psi_{\text{target}}\rangle|^2 \quad (15)$$

is taken with respect to the most likely final cat state $\hat{a}^{K/2-k}|+\rangle_K$, not restricted to $|+\rangle$.

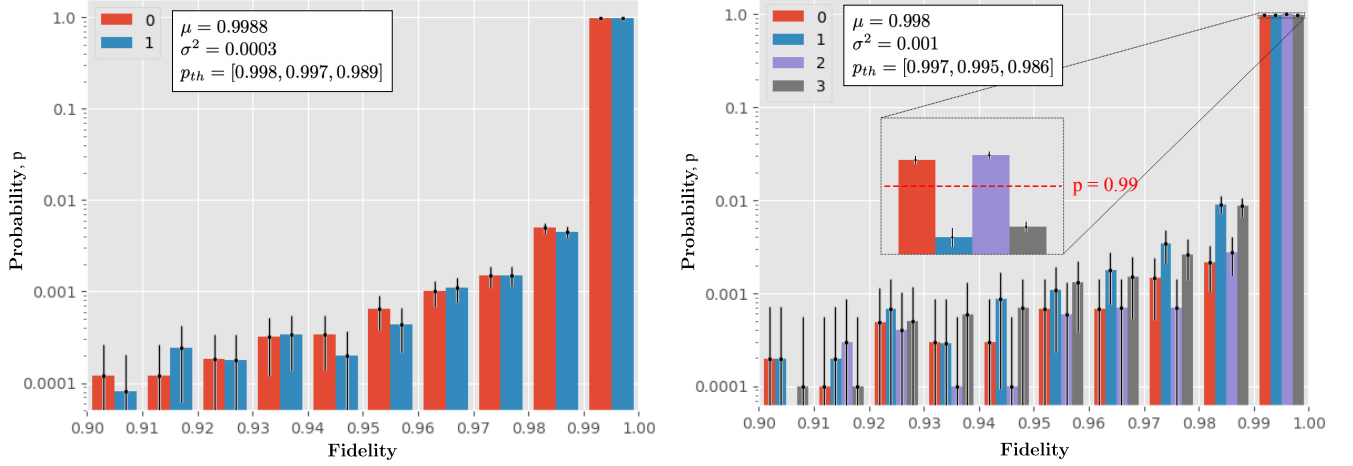


FIG. 3. Modular Photon Number Measurement shown in Figure 1 (c). Final state fidelities and their probabilities, with a probe cat state and a target coherent state of double amplitude. Error bars represent Wilson score 95% confidence intervals. Threshold probabilities are given for fidelities above 0.9, 0.95 and 0.99 respectively. Histogram bars correspond to measurement outcome indices, as sketched in Figure 2. **(Left)** Measuring the photon number mod 2, using a probe cat state with 2 coherent state components and $\alpha = 4$, and heterodyne local oscillators with amplitude $\beta = 6$. 10^5 samples taken. **(Right)** Measuring the photon number mod 4, using a probe cat state with 4 coherent state components and $\alpha = 12$, and heterodyne local oscillators of amplitude $\beta = 8$. 4×10^4 samples taken. **(Inset)** The 4-component results display a statistically significant difference in high-fidelity probabilities for even and odd indices, located either side of $p = 0.99$.

2. Relative Phases in Tele-correction

While the relative phases of the YS states can be corrected in modular photon number measurements, it may be expected that they would remain detrimental in tele-correction as these states do not have the photon number distribution of true cat code states. This turns out not to be the case; below we explore the performance of tele-correction by contrasting approximate preparation of cat states with the direct use of the YS states in the tele-correction circuit.

When a displacement is applied to a YS state, the form of the photon number distribution is altered and can display periodic behaviour [54]. A straightforward approach to cat state generation might be to optimise this distribution so that the bulk of the population exists in a particular modular subspace of the Fock states.

One way to look at the effect of a small displacement is through the additional relative phases introduced between coherent components, due to the relationship

$$\hat{D}(\alpha)\hat{D}(\sigma) = e^{i\text{Im}(\alpha\sigma^*)}\hat{D}(\alpha + \sigma). \quad (16)$$

Consider a simple, two-component cat state where both components lie along the real axis. The largest relative phase shift for a given $|\sigma|$ is achieved in this case with a displacement along the imaginary axis. Since the relative phase between components as a result of the YS method is $e^{i\pi/2}$, from Equation (12), this relative phase is corrected when $2\alpha\sigma = \pm i\pi/2$. Assuming the components of the state are widely separated ($\alpha \gg 1$), the fidelity with the target state after such a shift becomes $e^{-|\sigma|^2}$, which

highlights a trade-off in the shift magnitude between the phase correction and the component-wise state overlap. Similarly, the relative phases for the four-component case are

$$\frac{3\pi}{4}, \quad 0, \quad -\frac{\pi}{4}, \quad 0. \quad (17)$$

Components along the imaginary axis are equal, while the components along the real axis differ by π . We can manipulate these pairs independently with the real and imaginary components of σ . Identify the pair along the real axis with the logical $|+\rangle$ state, and that along the imaginary axis with the logical $|-\rangle$ state. Applying a displacement along the imaginary axis with amplitude $2\alpha\sigma = \pm i\pi$ results in an approximate logical state $|-\rangle + e^{\mp i\pi/4}|+\rangle$. The fidelity for large α is again $e^{-|\sigma|^2}$.

As the number of coherent state components increases, the number of degrees of freedom in their relative phases exceeds the two degrees of freedom available in a displacement. The consequence, as depicted in Figure 4, is that the overlap with any logical state restricted to a modular photon number subspace must decrease. By contrast, tele-correction involving YS states is not sensitive to these additional degrees of freedom; it may always be viewed as a combination of modular photon number measurements.

If the YS state is used as the input to the first rail in Figure 1 (a), then the first controlled rotation and measurement is a direct copy of the photon number measurement circuit in Figure 1 (c) with the second rail as the target. The stable performance of the tele-correction

scheme in this situation under measurement error is verified in the results of Figure 5. On the other hand, if the YS state is used as the input to the second rail of the tele-correction circuit, we may interpret the combination

$$\frac{1}{\sqrt{\mathcal{N}}} \sum_{n,n'} \left[\frac{\beta^{a_{n,\mu}K/2}}{\sqrt{(a_{n,\mu}K/2)!}} \frac{\delta^{b_{n',\nu}K'/2}}{\sqrt{(b_{n',\nu}K'/2)!}} \right] |a_{n,\mu}K/2\rangle \otimes \left[\sum_{m=1}^N e^{i\xi_m} | -\alpha e^{i\phi_m} e^{-i\frac{2\pi}{N}(a_{n,\mu}+b_{n',\nu})} \rangle \right] \otimes |b_{n',\nu}K'/2\rangle, \quad (18)$$

for $a_{n,\mu} = 2n + \mu$, $b_{n',\nu} = 2n' + \nu$, some normalisation constant \mathcal{N} and $\mu, \nu \in \{0, 1\}$. The relative phases are again inherited sequentially by the Fock states in the modular subspace, but in this case a cross-Kerr interaction,

$$e^{i\frac{4\pi}{K^2N}\hat{n}_1^2} e^{i\frac{4\pi}{K'^2N}\hat{n}_2^2} e^{i\frac{8\pi}{KK'N}\hat{n}_1\hat{n}_2}, \quad (19)$$

is required to remove the quadratic dependence.

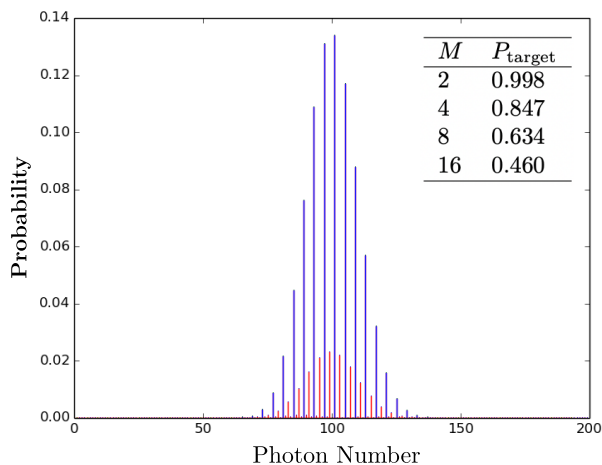


FIG. 4. Example photon number distribution for a displaced Yurke-Stoler state with target photon numbers separated in steps of $N = 4$. Parameters are $\alpha = 10$, $\sigma = 0.19 (N/\alpha)$. The modular photon number subspace with the maximum probability is shown in blue, with the remainder of the population in red. **(Inset)** The maximum probability P_{target} , numerically optimised, of measuring any single photon number outcome modulo M , for several M and $\alpha = 10$.

IV. DISCUSSION

In this work, we considered the component elements of the tele-correction circuit for rotationally symmetric Bosonic codes. Broadening the class of states allowed as ancillary inputs, we observed that states generated via

of both controlled rotations and the central measurement together as a measurement of the modular sum of photon numbers in the first and third rails. The resultant state in this case, prior to measurement, would be

a generalised Yurke-Stoler procedure [54] may be considered valid ancillary states, despite having population over the entire Fock state distribution. In support, we present randomised numerical samples that demonstrate robust output state fidelities in two instances: When tele-correction subcircuits are used to modify state amplitudes, and when Yurke-Stoler states are chosen as inputs for tele-correction.

One limitation of our results is the absence of loss errors in our analysis. It is well documented that in using Bosonic codes we must accept a trade-off and make a balanced choice of α to effectively reduce back-action and stabilise both loss and phase errors [59, 75, 81]. The main thrust of our paper has been the suitability of the Yurke-Stoler state structure for tele-correction. However, in proposing many-component states as a bridge for non-linear interactions we have also implicitly introduced a further trade-off between the number of components, the measurement error, and the photon loss rate (which increases with α). The Yurke-Stoler states, like coherent states, contain all Fock components. It would be interesting to see, in light of their unique phase structure, just where the balance between loss and measurement error might lie for these states. Further, while we have looked at this preparation scheme mainly in comparison to direct cross-Kerr and displacement operator approaches, the impact of timing inaccuracy, parameter drift and mid-evolution decay remain unclear.

We saw in Figure 3 that the modular photon number measurement could be used to turn a coherent state into a cat state, but these circuits are more broadly capable of conversion between code states of any amplitude and number of components. Where non-linear interaction strength is a key limiting factor, we propose using many-component Yurke-Stoler states as mediating ancillae to shorten interactions times for such inter-conversion, facilitating ancillary state generation and repeated correction.

ACKNOWLEDGMENTS

This work was supported by the UK EPSRC through EP/Y004752/1, EP/W032643/1, EP/Z53318X/1 and the National Research Foundation of Korea (NRF) grant

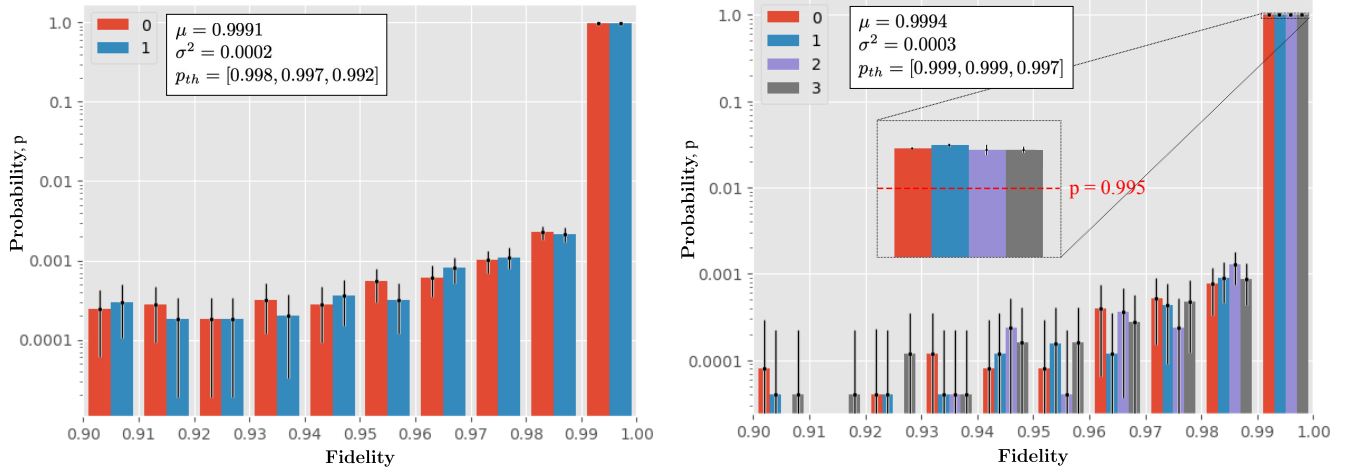


FIG. 5. Tele-correction as shown in Figure 1 (a), with a Yurke-Stoler input state to the first rail. These states are displaced prior to correction, to maximise the amplitude of the $|+\rangle$ state relative to the $|-\rangle$ state. Final state fidelities and their probabilities. Error bars represent Wilson score 95% confidence intervals. Threshold probabilities are given for fidelities above 0.9, 0.95 and 0.99 respectively. Histogram bars correspond to measurement outcome indices, as sketched in Figure 2. **(Left)** Input and ancillary states have 2 coherent state components and $\alpha = 3$, with heterodyne local oscillators of amplitude $\beta = 10$. 10^5 samples taken. **(Right)** Input and ancillary states have 4 coherent state components and $\alpha = 4$, with heterodyne local oscillators of amplitude $\beta = 10$. 10^5 samples taken. **(Inset)** Unlike for the modular photon number measurement of Figure 3, the 4-component results do not display a statistically significant difference in high-fidelity probabilities for even and odd outcomes.

funded by the Korea government (MSIT) (No. RS-2024-00413957). NL, SN, WJM and KN were supported in part from the Moonshot R&D Program Grants JPMJMS2061 & JPMJMS226C, COI-NEXT under Grant

No. JPMJPF2221, and the JSPS KAKENHI Grant No. 21H04880. SN further acknowledges support from JSPS KAKENHI Grant Number JP22KJ1436.

-
- [1] P. Shor, in *Proceedings 35th Annual Symposium on Foundations of Computer Science* (IEEE Comput. Soc. Press, Santa Fe, NM, USA, 1994) pp. 124–134.
 - [2] D. Jennings, M. Lostaglio, R. B. Lowrie, S. Pallister, and A. T. Sornborger, The cost of solving linear differential equations on a quantum computer: Fast-forwarding to explicit resource counts (2023), arXiv:2309.07881 [quant-ph].
 - [3] K. Zaman, A. Marchisio, M. A. Hanif, and M. Shafique, A Survey on Quantum Machine Learning: Current Trends, Challenges, Opportunities, and the Road Ahead (2023), arXiv:2310.10315 [quant-ph].
 - [4] D. Pan, G.-L. Long, L. Yin, Y.-B. Sheng, D. Ruan, S. X. Ng, J. Lu, and L. Hanzo, IEEE Communications Surveys & Tutorials **26**, 1898 (2024).
 - [5] S. Pirandola, U. L. Andersen, L. Banchi, M. Berta, D. Bunandar, R. Colbeck, D. Englund, T. Gehring, C. Lupo, C. Ottaviani, J. L. Pereira, M. Razavi, J. Shamsul Shaari, M. Tomamichel, V. C. Usenko, G. Vallone, P. Villoresi, and P. Wallden, Advances in Optics and Photonics **12**, 1012 (2020).
 - [6] M. A. Taylor and W. P. Bowen, Physics Reports **615**, 1 (2016).
 - [7] Y. Kim, A. Eddins, S. Anand, K. X. Wei, E. Van Den Berg, S. Rosenblatt, H. Nayfeh, Y. Wu, M. Zale-
tel, K. Temme, and A. Kandala, Nature **618**, 500 (2023).
 - [8] F. Arute, K. Arya, R. Babbush, D. Bacon, J. C. Bardin, R. Barends, R. Biswas, S. Boixo, F. G. S. L. Brandao, D. A. Buell, B. Burkett, Y. Chen, Z. Chen, B. Chiaro, R. Collins, *et al.*, Nature **574**, 505 (2019).
 - [9] F. Pan and P. Zhang, Simulating the Sycamore quantum supremacy circuits (2021), arXiv:2103.03074 [physics, physics:quant-ph].
 - [10] J. Tindall, M. Fishman, E. M. Stoudenmire, and D. Sels, PRX Quantum **5**, 010308 (2024).
 - [11] H.-J. Liao, K. Wang, Z.-S. Zhou, P. Zhang, and T. Xiang, Simulation of IBM’s kicked Ising experiment with Projected Entangled Pair Operator (2023), arXiv:2308.03082 [cond-mat, physics:quant-ph].
 - [12] T. Begušić and G. K.-L. Chan, Fast classical simulation of evidence for the utility of quantum computing before fault tolerance (2023), arXiv:2306.16372 [quant-ph].
 - [13] L. Clinton, T. Cubitt, B. Flynn, F. M. Gambetta, J. Klassen, A. Montanaro, S. Piddock, R. A. Santos, and E. Sheridan, Nature Communications **15**, 211 (2024).
 - [14] N. C. Rubin, D. W. Berry, A. Kononov, F. D. Malone, T. Khattar, A. White, J. Lee, H. Neven, R. Babbush, and A. D. Baczewski, Proceedings of the National Academy of Sciences **121**, e2317772121 (2024).
 - [15] C. Gidney and M. Ekerå, Quantum **5**, 433 (2021).

- [16] D. Aharonov, M. Ben-Or, R. Impagliazzo, and N. Nisan, Limitations of Noisy Reversible Computation (1996), arXiv:quant-ph/9611028.
- [17] A. Müller-Hermes, D. Stilck França, and M. M. Wolf, Journal of Mathematical Physics **57**, 022202 (2016).
- [18] R. Raussendorf, Philosophical Transactions of the Royal Society A: Mathematical, Physical and Engineering Sciences **370**, 4541 (2012).
- [19] E. Campbell, Nature Reviews Physics **6**, 160 (2024).
- [20] C. Ryan-Anderson, J. G. Bohnet, K. Lee, D. Gresh, A. Hankin, J. P. Gaebler, D. Francois, A. Chernoguzov, D. Lucchetti, N. C. Brown, T. M. Gatterman, S. K. Halit, K. Gilmore, J. A. Gerber, B. Neyenhuis, D. Hayes, and R. P. Stutz, Physical Review X **11**, 041058 (2021).
- [21] N. Sundaresan, T. J. Yoder, Y. Kim, M. Li, E. H. Chen, G. Harper, T. Thorbeck, A. W. Cross, A. D. Córcoles, and M. Takita, Nature Communications **14**, 2852 (2023).
- [22] D. Bluvstein, S. J. Evered, A. A. Geim, S. H. Li, H. Zhou, T. Manovitz, S. Ebadi, M. Cain, M. Kalinowski, D. Hangleiter, J. P. B. Ataides, N. Maskara, I. Cong, X. Gao, P. S. Rodriguez, T. Karolyshyn, G. Semeghini, M. J. Gullans, M. Greiner, V. Vuletić, and M. D. Lukin, Nature 10.1038/s41586-023-06927-3 (2023).
- [23] Google Quantum AI, R. Acharya, I. Aleiner, R. Allen, T. I. Andersen, M. Ansmann, F. Arute, K. Arya, A. Asfaw, J. Atalaya, R. Babbush, D. Bacon, J. C. Bardin, J. Basso, A. Bengtsson, *et al.*, Nature **614**, 676 (2023).
- [24] R. K. Naik, N. Leung, S. Chakram, P. Groszkowski, Y. Lu, N. Earnest, D. C. McKay, J. Koch, and D. I. Schuster, Nature Communications **8**, 1904 (2017).
- [25] C. Duckering, J. M. Baker, D. I. Schuster, and F. T. Chong, in *2020 53rd Annual IEEE/ACM International Symposium on Microarchitecture (MICRO)* (IEEE, Athens, Greece, 2020) pp. 173–185.
- [26] C. Chamberland, K. Noh, P. Arrangoiz-Arriola, E. T. Campbell, C. T. Hann, J. Iverson, H. Putterman, T. C. Bohdanowicz, S. T. Flammia, A. Keller, G. Refael, J. Preskill, L. Jiang, A. H. Safavi-Naeini, O. Painter, and F. G. Brandão, PRX Quantum **3**, 010329 (2022).
- [27] K. Noh, C. Chamberland, and F. G. Brandão, PRX Quantum **3**, 010315 (2022).
- [28] Y. Xu, Y. Wang, E.-J. Kuo, and V. V. Albert, PRX Quantum **4**, 020342 (2023).
- [29] K. Azuma, S. E. Economou, D. Elkouss, P. Hilaire, L. Jiang, H.-K. Lo, and I. Tzitrin, Reviews of Modern Physics **95**, 045006 (2023).
- [30] F. Rozpędek, K. P. Seshadreesan, P. Polakos, L. Jiang, and S. Guha, Physical Review Research **5**, 043056 (2023).
- [31] P.-Z. Li, J. Dias, W. J. Munro, P. Van Loock, K. Nemoto, and N. Lo Piparo, Advanced Quantum Technologies **7**, 2300252 (2024).
- [32] S. L. Braunstein, Nature **394**, 47 (1998).
- [33] P. T. Cochrane, G. J. Milburn, and W. J. Munro, Physical Review A **59**, 2631 (1999).
- [34] D. Gottesman, A. Kitaev, and J. Preskill, Physical Review A **64**, 012310 (2001).
- [35] G. Pantaleoni, B. Q. Baragiola, and N. C. Menicucci, Physical Review Letters **125**, 040501 (2020).
- [36] A. L. Grimsmo, J. Combes, and B. Q. Baragiola, Physical Review X **10**, 011058 (2020).
- [37] Y. Shi, C. Chamberland, and A. Cross, New Journal of Physics **21**, 093007 (2019).
- [38] A. M. Steane, Nature **399**, 124 (1999).
- [39] E. Knill, Fault-Tolerant Postselected Quantum Computation: Schemes (2004), arXiv:quant-ph/0402171.
- [40] W. J. Munro, G. J. Milburn, and B. C. Sanders, Physical Review A **62**, 052108 (2000).
- [41] H. Jeong and M. S. Kim, Physical Review A **65**, 042305 (2002).
- [42] T. C. Ralph, A. Gilchrist, G. J. Milburn, W. J. Munro, and S. Glancy, Physical Review A **68**, 042319 (2003).
- [43] A. Ourjoumtsev, R. Tualle-Brouri, J. Laurat, and P. Grangier, Science **312**, 83 (2006).
- [44] A. Ourjoumtsev, H. Jeong, R. Tualle-Brouri, and P. Grangier, Nature **448**, 784 (2007).
- [45] M. Takeoka and M. Sasaki, Physical Review A **75**, 064302 (2007).
- [46] A. P. Lund, T. C. Ralph, and H. L. Haselgrove, Physical Review Letters **100**, 030503 (2008).
- [47] H. Takahashi, K. Wakui, S. Suzuki, M. Takeoka, K. Hayasaka, A. Furusawa, and M. Sasaki, Physical Review Letters **101**, 233605 (2008).
- [48] C. Arenz, C. Cormick, D. Vitali, and G. Morigi, Journal of Physics B: Atomic, Molecular and Optical Physics **46**, 224001 (2013).
- [49] M. J. Everitt, T. P. Spiller, G. J. Milburn, R. D. Wilson, and A. M. Zagoskin, Frontiers in ICT **1**, 10.3389/fict.2014.00001 (2014).
- [50] S. Puri, S. Boutin, and A. Blais, npj Quantum Information **3**, 18 (2017).
- [51] B. Yurke and D. Stoler, Physical Review Letters **57**, 13 (1986).
- [52] B. Sherman and G. Kurizki, Physical Review A **45**, R7674 (1992).
- [53] B. M. Garraway, B. Sherman, H. Moya-Cessa, P. L. Knight, and G. Kurizki, Physical Review A **49**, 535 (1994).
- [54] K. S. Lee, M. S. Kim, and V. Büzek, Journal of the Optical Society of America B **11**, 1118 (1994).
- [55] G. S. Agarwal and P. K. Pathak, Physical Review A **70**, 053813 (2004).
- [56] J. Hastrup, J. S. Neergaard-Nielsen, and U. L. Andersen, Optics Letters **45**, 640 (2020).
- [57] R. Nehra, M. Eaton, O. Pfister, and A. Marandi, in *Conference on Lasers and Electro-Optics* (Optica Publishing Group, San Jose, California, 2022) p. FF2I.2.
- [58] S. Glancy, H. M. Vasconcelos, and T. C. Ralph, Physical Review A **70**, 022317 (2004).
- [59] L. Li, C.-L. Zou, V. V. Albert, S. Muralidharan, S. M. Girvin, and L. Jiang, Physical Review Letters **119**, 030502 (2017).
- [60] J. Guillaud and M. Mirrahimi, Physical Review X **9**, 041053 (2019).
- [61] J. Guillaud, J. Cohen, and M. Mirrahimi, SciPost Physics Lecture Notes **72** (2023).
- [62] A. S. Darmawan, B. J. Brown, A. L. Grimsmo, D. K. Tuckett, and S. Puri, PRX Quantum **2**, 030345 (2021).
- [63] K. Fukui, A. Tomita, A. Okamoto, and K. Fujii, Physical Review X **8**, 021054 (2018).
- [64] C. Vuillot, H. Asasi, Y. Wang, L. P. Pryadko, and B. M. Terhal, Physical Review A **99**, 032344 (2019).
- [65] K. Noh and C. Chamberland, Physical Review A **101**, 012316 (2020).
- [66] M. V. Larsen, C. Chamberland, K. Noh, J. S. Neergaard-Nielsen, and U. L. Andersen, PRX Quantum **2**, 030325 (2021).
- [67] L. Hänggli, M. Heinze, and R. König, Physical Review A **102**, 052408 (2020).

- [68] T. Itogawa, Y. Takada, Y. Hirano, and K. Fujii, Even more efficient magic state distillation by zero-level distillation (2024), arXiv:2403.03991 [quant-ph].
- [69] C. Gidney, N. Shutty, and C. Jones, Magic state cultivation: Growing T states as cheap as CNOT gates (2024), arXiv:2409.17595 [quant-ph].
- [70] Z. Leghtas, G. Kirchmair, B. Vlastakis, R. J. Schoelkopf, M. H. Devoret, and M. Mirrahimi, Physical Review Letters **111**, 120501 (2013).
- [71] M. Mirrahimi, Z. Leghtas, V. V. Albert, S. Touzard, R. J. Schoelkopf, L. Jiang, and M. H. Devoret, New Journal of Physics **16**, 045014 (2014).
- [72] N. Ofek, A. Petrenko, R. Heeres, P. Reinhold, Z. Leghtas, B. Vlastakis, Y. Liu, L. Frunzio, S. M. Girvin, L. Jiang, M. Mirrahimi, M. H. Devoret, and R. J. Schoelkopf, Nature **536**, 441 (2016).
- [73] A. Grimm, N. E. Frattini, S. Puri, S. O. Mundhada, S. Touzard, M. Mirrahimi, S. M. Girvin, S. Shankar, and M. H. Devoret, Nature **584**, 205 (2020).
- [74] V. V. Albert, C. Shu, S. Krastanov, C. Shen, R.-B. Liu, Z.-B. Yang, R. J. Schoelkopf, M. Mirrahimi, M. H. Devoret, and L. Jiang, Physical Review Letters **116**, 140502 (2016).
- [75] T. Hillmann, F. Quijandría, A. L. Grimsom, and G. Ferrini, PRX Quantum **3**, 020334 (2022).
- [76] C. Oh, C. Lee, C. Rockstuhl, H. Jeong, J. Kim, H. Nha, and S.-Y. Lee, npj Quantum Information **5**, 10 (2019).
- [77] L. S. Martin, W. P. Livingston, S. Hacohe-Gourgy, H. M. Wiseman, and I. Siddiqi, Nature Physics **16**, 1046 (2020).
- [78] H. Schöpf and P. Supancic, The Mathematica Journal **16**, 10.3888/tmj.16-11 (2014).
- [79] S. W. Smith, *Digital Signal Processing* (Newnes, Elsevier, 2003).
- [80] B. C. Berndt and R. J. Evans, Bulletin of the American Mathematical Society **5**, 107 (1981).
- [81] V. V. Albert, K. Noh, K. Duivenvoorden, D. J. Young, R. T. Brierley, P. Reinhold, C. Vuillot, L. Li, C. Shen, S. M. Girvin, B. M. Terhal, and L. Jiang, Physical Review A **97**, 032346 (2018).